Measurement Uncertainty Analysis in Determining Adiabatic Film Cooling Effectiveness by Using Pressure Sensitive Paint Technique

Blake Johnson[1]
Department of Aerospace Engineering,
Iowa State University,
2271 Howe Hall, Room 1200,
Ames, IA 50011-2217

Hui Hu[2]
Fellow ASME
Department of Aerospace Engineering,
Iowa State University,
2271 Howe Hall, Room 1200,
Ames, IA 50011-2217
e-mail: huhui@iastate.edu

While pressure sensitive paint (PSP) technique has been widely used to measure adiabatic film cooling effectiveness distributions on the surfaces of interest based on a mass transfer analog to traditional thermal-based measurements, very little can be found in literature to provide a comprehensive analysis on the uncertainty levels of the measured film cooling effectiveness distributions derived from PSP measurements. In the present study, a detailed analysis is performed to evaluate the effects of various associated uncertainties in the PSP measurements on the measured film cooling effectiveness distributions over the surfaces of interest. The experimental study is conducted in a low-speed wind tunnel under an isothermal condition. While airflow is used to represent the "hot" mainstream flow, an oxygen-free gas, i.e., carbon dioxide (CO_2) gas with a density ratio of $DR = 1.5$ for the present study, is supplied to simulate the "coolant" stream for the PSP measurements to map the adiabatic film cooling effectiveness distribution over a flat test plate with an array of five cylindrical coolant holes at a span-wise spacing of three diameters center-to-center. A comprehensive analysis was carried out with focus on the measurement uncertainty and process uncertainty for the PSP measurements to determine the film cooling effectiveness distributions over the surface of interest. The final analysis indicates that the total uncertainty in the adiabatic film cooling effectiveness measurements by using the PSP technique depends strongly on the local behavior of the mixing process between the mainstream and coolant flows. The measurement uncertainty is estimated as high as 5% at the near field behind the coolant holes. In the far field away from the coolant holes, the total measurement uncertainty is found to be more uniform throughout the measurement domain and generally lower than those in the near field at about 3%.
[DOI: 10.1115/1.4033506]

Introduction

Because of the widespread usage of gas turbine engines in fields such as aircraft propulsion and electrical power generation, every innovation that improves the performance of gas turbines, if even by marginal increments, may lead to great value of savings. Maximizing the performance and efficiency of gas turbines is best achieved by elevating the turbine inlet temperature. As the temperature has increased, various advanced technologies have been developed to protect the metallic turbine components from damage and failure. Some of these developments include manufacturing turbine blades from single crystals, the addition of ceramic thermal barrier coatings, improved internal cooling of turbine blades, and the fluid-based external protection of turbine blades via film cooling technologies.

While accurate measurements of film cooling effectiveness on the surface of interest are very critical to evaluate various film cooling designs for improved protection of the critical portions of turbine blades from harsh environments, they have been proved particularly challenging from the experimental standpoint due to difficulties that arise from the effects of heat conduction within the solid test materials of the turbine blades [1,2]. Extensive research has been conducted to resolve the effects of heat conduction within the solid surfaces under question [3,4]. Computational fluid dynamics models have had limited success recreating the measurements of experimental studies, and it is suspected that the main difficulty lies in matching the heat conduction conditions appropriately [5,6]. Common thermal measurement techniques that have been employed include direct measurements of the surface temperature through the use of thermocouples [4], infrared thermography [7], laser induced fluorescence [8], and the temperature-sensitive paint [3,9] techniques. To provide the best-possible data for quantitative comparison to numerical simulations, it is desirable that the experimental measurements be able to achieve truly adiabatic measurements of the film cooling effectiveness.

Alternative techniques, based on mass transfer analogy rather than conducting temperature measurements, have also been suggested for quantitative measurements of adiabatic film cooling effectiveness over the surfaces of interest for film cooling studies. The techniques are usually performed under isothermal conditions, and are based upon measurements of concentrations of different gas species. Researchers have used gas sampling to determine the gas concentrations [10] and, in recent years, have taken advantage of the function of PSPs to measure species concentrations optically [11–14]. Since the experiments were able to be performed at isothermal conditions, the measurement results

[1]Present address: Department of Mechanical Science and Engineering, University of Illinois at Urbana-Champaign, Urbana, IL.
[2]Corresponding author.
Contributed by the International Gas Turbine Institute (IGTI) of ASME for publication in the Journal of Turbomachinery. Manuscript received August 18, 2015; final manuscript received April 15, 2016; published online June 14, 2016. Assoc. Editor: David G. Bogard.

are free from the heat conduction-related measurement errors that are frequently encountered in conventional heat transfer-based experiments by measuring surface temperature to determine the adiabatic film cooling effectiveness on the surface of interest.

While a number of experimental studies have been conducted in recent years using the PSP technique to achieve quantitative film cooling effectiveness measurements with mass transfer analogy [11–17], the PSP technique is still a fairly new technique to measure film cooling effectiveness, in comparison to conventional temperature-based methods. Much work is still required to validate the reliability of PSP-based measurements in order to make the PSP technique as an effective and robust experimental tool for film cooling studies. More recently, Johnson et al. [18] conducted an experimental study to compare the film cooling effectiveness data derived from PSP measurements quantitatively against those of the temperature-based measurements under the same or comparable test conditions. It was found that, while the measured film cooling effectiveness with PSP technique agrees well in general with that of Baldauf et al. [2] with an IR thermometry technique at comparable test conditions, some minor differences can also be identified based on the back-to-back comparison of the two measurement results. The discrepancies between the two measurements were attributed to the fundamental differences between the two measurement techniques. The slightly higher cooling effectiveness with a wider-spanning footprint of the coolant flow revealed in the IR thermometry measurements was suggested due to the effects of heat conduction through the test model, particularly in the lateral direction.

While the measurement uncertainty analysis of the film cooling effectiveness derived from temperature-based measurements has been well explored [1,2,9], very little can be found in literature about the measurement uncertainty estimation of the film cooling effectiveness derived from the PSP measurements. In the present study, a detailed uncertainty analysis is performed to evaluate the effects of various associated uncertainties in PSP measurements on the measured film cooling effectiveness distributions over the surfaces of interest. The experimental study was conducted in a low-speed wind tunnel under an isothermal condition. While airflow was used to represent the hot mainstream flow, CO_2 gas with a density ratio of DR = 1.5 was supplied to simulate the coolant stream for the PSP measurements to map the adiabatic film cooling effectiveness distribution over a flat test plate with an array of five cylindrical coolant holes at a span-wise spacing of three diameters center-to-center. A comprehensive analysis was carried out with focus on the measurement uncertainty and process uncertainty for the PSP measurements to determine the film cooling effectiveness distributions over the surface of interest. Throughout this work, the measurement uncertainty is a reference of the 95% confidence interval based on approximately two standard deviations. To the best knowledge of the authors, this is among first efforts of its nature, in addition to the more recent work done by Natsui et al. [19], who performed a similar analysis that also presented data related to the repeatability of their measurements. They presented uncertainty maps in the effectiveness that varied from roughly ± 0.01 to nearly ± 0.05 in the area greater than 30 diameters from the injection hole. The findings of the present study are believed to be very helpful to validate the reliability of the PSP-based measurements and to make PSP technique as an effective and robust experimental tool for film cooling studies.

Technical Basics of the PSP Technique

PSP consists of a gas-permeable polymeric paint binder that contains certain luminescent molecules that are sensitive to diatomic oxygen [19]. Oxygen can interact with the molecule so that the transition to the ground state is radiationless, in a process known as oxygen quenching, whereby the emission intensity is inversely related to the partial pressure P_{O_2} of O_2 gas. The intensity decrease can be described by the well-known Stern–Volmer equation

$$\frac{I_0}{I_{O_2}} = 1 + K_{SV} P_{O_2} \tag{1}$$

where I_0 is the reference intensity of the PSP emission, I_{O_2} is the emission intensity of the PSP, and K_{SV} is a calibration-determined constant. In practice, a calibration curve of higher polynomial order is typically used.

Because the volume fraction of oxygen in air is fixed at about 20%, higher partial pressure or concentration of oxygen would indicate higher local air pressure. The air pressure distribution on the painted surface can be determined based on the intensity distribution of the acquired image of the oxygen sensitive molecules. Generally, the luminescent response of PSP is small enough that it is only useful for measurements of pressure in flows where pressure gradients are large, such as high-speed compressible flows. It should be noted that, because its operation is based on the presence of O_2 gas, PSP can alternatively be used to detect the concentration of gas species that are void of O_2, even in low-speed incompressible flows. In the present study, the PSP technique is used to map the oxygen concentration distribution over a test surface protected an oxygen-free gas (e.g., Nitrogen or CO_2) in order to derive adiabatic film cooling effectiveness distributions on the surface of interest based on a mass transfer analog to traditional thermal-based measurements. While Liu and Sullivan [20] provided a comprehensive uncertainty analysis of PSP measurements to quantify surface pressure distributions of test models in air flows, the focus of the present study is on the uncertainty levels of the measured film cooling effectiveness distributions derived from the PSP measurements.

Cooling Effectiveness Measurements by Using PSP Technique

Traditionally, the adiabatic film cooling effectiveness is defined based on temperature measurements, and is expressed as

$$\eta = \frac{T_\infty - T_{aw}}{T_\infty - T_c} \tag{2}$$

where T_{aw} is the adiabatic wall temperature, T_∞ is the mainstream temperature, and T_c is the temperature of the coolant. As described above, the primary challenge associated with the temperature-based method is in measuring the true adiabatic wall temperature despite the physical reality of heat conduction within the test model.

Instead of conducting heat transfer experiments to measure the temperature variations on the surface of interest, the film cooling effectiveness can also be measured quantitatively by performing "cold" experiments at isothermal conditions with the PSP technique through use of a mass transfer analogy [11,14,17,21]. The mass transfer analogy works whereby the film cooling effectiveness is cast in terms of the oxygen concentrations C_i against the protected surface measured by using the PSP technique

$$\eta = \frac{C_\infty - C_{wall}}{C_\infty - C_c} \tag{3}$$

where C_{wall} is the O_2 concentration at the wall and the other subscripts are as for the thermal measurements. Note that $C_c = 0$ for choice of a pure coolant gas that contains no free O_2. If there is no significant density difference between the coolant gas and the mainstream gas, then Eq. (3) could be written in terms of the partial pressures of O_2 present in each stream and in at the wall

$$\eta = \frac{(P_{O_2})_{air} - (P_{O_2})_{wall}}{(P_{O_2})_{air} - (P_{O_2})_c} \tag{4}$$

which is a form that is measurable using PSP. The particular method necessary to obtain the partial pressures requires a series of four image captures of the PSP emission radiation.

Charbonnier et al. [13] suggested an appropriate way to relate the film cooling effectiveness measurements when the measurement technique detects the partial pressure of a gas species, rather than the concentration, provided the coolant gas contains no O_2. They suggested that the film cooling effectiveness is a function of not only the partial pressure ratio, but also of the molecular weight ratio, $MW \equiv M_{gas}/M_{air}$, of the coolant gas to the mainstream gas (air in this study), which can be expressed as

$$\eta = 1 - \frac{1}{\left[\left(P_{\text{air jet}}/P_{\text{gas jet}}\right) - 1\right]\text{MW} + 1} \tag{5}$$

where the terms in the pressure ratio here in the denominator in fact refer to the partial O_2 pressures of the air jet measurement case and the coolant gas measurement case. A similar expression was derived by Han and Rallabandi [22]. In order to arrive at this pressure ratio, the PSP technique is used in the following way:

$$\frac{P_{\text{gas}}}{P_{\text{air}}} = \frac{P_{\text{gas}}/P_{\text{ref}}}{P_{\text{air}}/P_{\text{ref}}} \tag{6}$$

where P_{ref} is the pressure of a reference condition convenient to the PSP technique, more specifically, the static pressure condition where the wind tunnel and coolant flows both are turned off, rendering the oxygen pressure acting on the PSP measurements equivalent to the static ambient component of that partial pressure. In order to measure the pressure ratios in the numerator and denominator of the above expression, PSP measurements are of the form

$$\frac{P_i}{P_{\text{ref}}} = f^{-1}\left(\frac{I_{\text{ref}} - I_b}{I_i - I_b}\right) = f^{-1}\left(I_i^*\right) \tag{7}$$

where i may refer to the air-as-coolant flow condition or the non-O_2-gas-as-coolant flow condition. I_{ref}, I_b, and I_i here refer to the digital camera measurements of image intensities for the reference nonflow condition (static with excitation light on), ambient-lighting-only nonflow condition (static with excitation light off), and the image intensities for the aforementioned coolant flow conditions, respectively. As a shorthand notation, I_i^* is used to represent a normalized image intensity ratio. Thus, the basic measurands for the PSP technique consist of a series of four images I_{ref}, I_b, I_{air}, and I_{gas}, each of which is the average of an ensemble of images.

Experimental Setup

PSP Calibration. Figure 1 shows the schematic of the experimental setup used in the present study for PSP calibration. A calibration cell with two chambers separated by a copper test plate was designed for the PSP calibration. The front of the test plate was painted with PSP, while the back of the test plate was exposed to an enclosed chamber through which coolant fluid was circulated. An external thermal regulator was used to circulate and control the temperature of the coolant. The frontal chamber has a silicon-quartz window through which the test plate was illuminated and imaged. The chamber is pressure-controlled and the pressure within the chamber was measured with a digital pressure transducer (DSA 3217 Module, Scanivalve Corp, 100 psi full-scale with ±0.05 psi accuracy). A K-type thermocouple and a reader with 0.1 °C resolution continuously monitored the temperature of the chamber. The thermocouple was moved throughout the calibration chamber to confirm uniformity of the temperature field throughout the calibration cell. Because the film cooling effectiveness measurements utilize a foreign gas with zero O_2 content to simulate the coolant flow, the PSP calibration procedure was performed with vacuum pressure. A vacuum pump was employed to depressurize the test cell for most of the range of the calibration while a continuous CO_2-flush was used to achieve a calibration point at true-zero O_2 pressure. A reference pressure of 1.0 atm (absolute) was used, which corresponds in the wind tunnel experiments to a condition of $\eta = 0$.

The PSP paint that was chosen for this experimental campaign is ISSI UniFIB due to its low stated temperature sensitivity (~0.5%/°C) and single-coat application. The paint has peak emission intensity at 650 nm upon illumination with 390 nm UV light. Imaging of the flow is accomplished through use of a 14-bit digital 2048 × 2048 pixel CCD array camera (PCO2000 monochrome) fitted with a long-pass filter with a 610 nm cutoff wavelength.

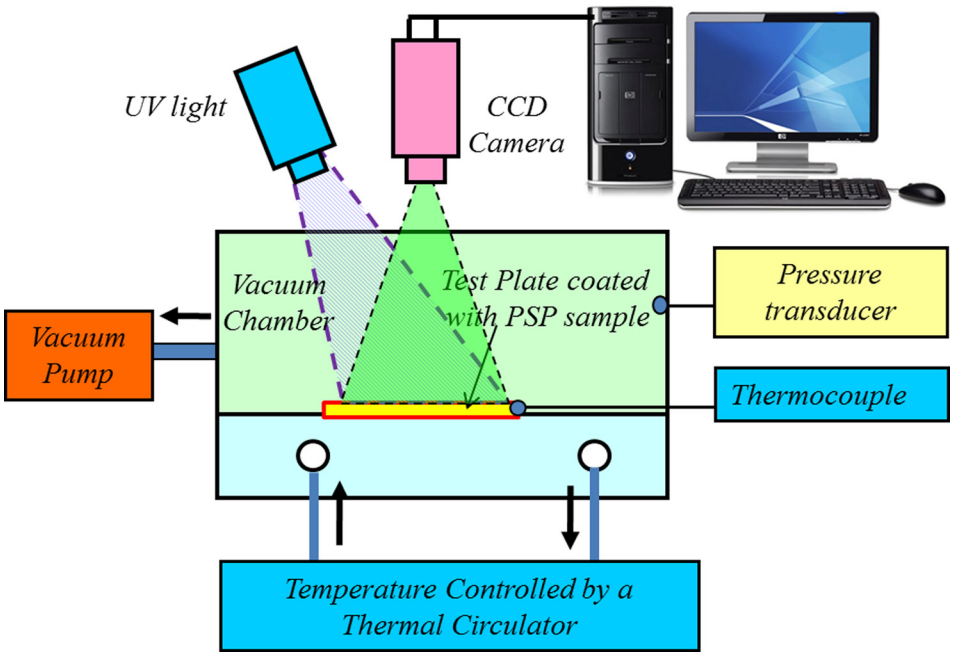

Fig. 1 Schematic layout for PSP calibration setup

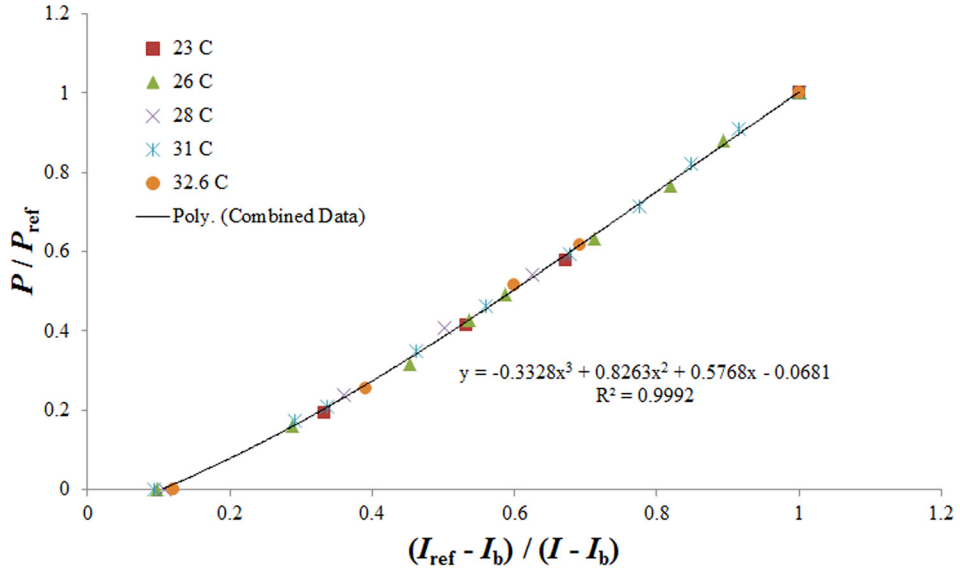

Fig. 2 PSP calibration curves in the range applicable for the film cooling effectiveness measurements

In the present study, PSP calibration was performed for a range of temperatures from 23.0 °C to 32.6 °C. For each temperature condition, all calibration points including the reference pressure were performed at a constant temperature. For example, all calibration data taken at 23.0 °C were normalized by reference conditions at 23.0 °C, calibration data taken at 28.0 °C were likewise normalized by reference conditions at 28.0 °C, and so on for the other temperature conditions. The camera was exposed for 45 ms per image over an ensemble of 3000 images per condition, during which the PSP sample was continuously excited. In order to limit effects of degradation of the PSP throughout the calibration process, the excitation light was immediately deactivated after each image acquisition phase. As shown clearly in Fig. 2, the PSP response, upon normalization by the appropriate condition, is independent of temperature. A similar feature of the PSP calibration curves was also found by Liu et al. [23].

Since each of the five temperature conditions yield very similar calibration curves, the 95% confidence interval of the calibration was estimated using the Student's t-distribution probability. Precision uncertainty of less than 0.9% deviation is observed for the full range of normalized intensities corresponding to the tested pressure range. The calibration curve that was found and used in this study is represented with a third-order polynomial

$$\frac{P_i}{P_{\text{ref}}} = -0.3328\left(\frac{I_{\text{ref}} - I_b}{I_i - I_b}\right)^3 + 0.8263\left(\frac{I_{\text{ref}} - I_b}{I_i - I_b}\right)^2 + 0.5768\left(\frac{I_{\text{ref}} - I_b}{I_i - I_b}\right) - 0.0681 \tag{8}$$

which closely resembles the calibration curve reported in Ref. [23], though the calibration coefficients are rather dissimilar.

Wind Tunnel Setup. In the present study, a low-speed open-circuit wind tunnel driven by a squirrel-cage fan provides the mainstream flow, while a secondary system that employs a reservoir of compressed gas is used for the coolant flow. Various oxygen-free gases (N_2, CO_2, SF_6, etc.) may be used as the coolant flow, depending on the desired density ratio, DR. The fan pushes the airflow through an initial diffuser to a series of flow conditioning devices that straighten the airflow and reduce the mainstream turbulence level. A contraction section that follows a fifth-order polynomial shape accelerates the airflow into the test section. The favorable pressure gradient through the contraction causes a thinning of the boundary layer that enters the test section, creating a plug-flow condition at the test section entrance from which the boundary layer develops. The test section has a cross-sectional area of 200 mm (w) × 125 mm (h) with a length of 300 mm (l) in the streamwise direction. The underside of the test section is open for the placement of the test plate.

Figure 3 shows schematically the experimental setup used in the present study. A flat test plate is designed to have an array of five cylindrical coolant holes of diameter $D = 5.0$ mm at an injection angle $\alpha = 30$ deg and a spanwise spacing of three diameters center-to-center. The test plate was made by a 3D printing process out of a hard plastic with its upper surface being carefully processed with fine sandpapers (i.e., up to 2000 grit) and specialty plastic polishes to achieve a very smooth, glossy finish. The test plate was attached and sealed to a plenum chamber through which the coolant gas passes before emitting from the coolant holes. The inlets of the coolant injection holes are fluted to allow smooth entry from the plenum and have a total axial length $L = 6D$, as measured from the outer entrance plane of the fluted inlets to the breakout plane at the upper surface of the test model. The axial centerlines of the coolant injection holes intersect the upper surface of the test plate at a distance $L = 115$ mm from the leading edge of the test plate. Thus, the boundary layer develops for a length of $22D$ before the mainstream flow encounters the coolant holes. In the present study, the velocity of the mainstream flow at the inlet of the test section was fixed at $U_\infty = 30$ m/s, the corresponding Reynolds number is $\text{Re} = 2.2 \times 10^5$, based on the distance between the leading edge of the test plate and the coolant injection hole.

The upper surface of the test plate is painted with the PSP. Upon the excitation of a UV light emitting diode (LED) lamp at the wavelength of 490 nm, the PSP emission is imaged with a 14-bit CCD camera (i.e., PCO2000 camera with 2048 × 2048 pixel in resolution) and long-pass filtered at 610 nm to isolate emission radiation from the UV excitation light. To reduce effects of camera noise on the data, averaging was performed on square groups of 9 × 9 pixels with 50% overlap (one data point every 4 pixels) to ensure complete sampling of the data. For the PSP measurements, the experiments typically have an image magnification of about 0.093 mm/pixel (or 10.7 pixels/mm), which results in a spatial resolution of $dx = dz = 0.37$ mm, or $0.074D$.

In the present study, the flowrate of the coolant flow stream was measured by using an Omega FMA-1600 series laminar flow

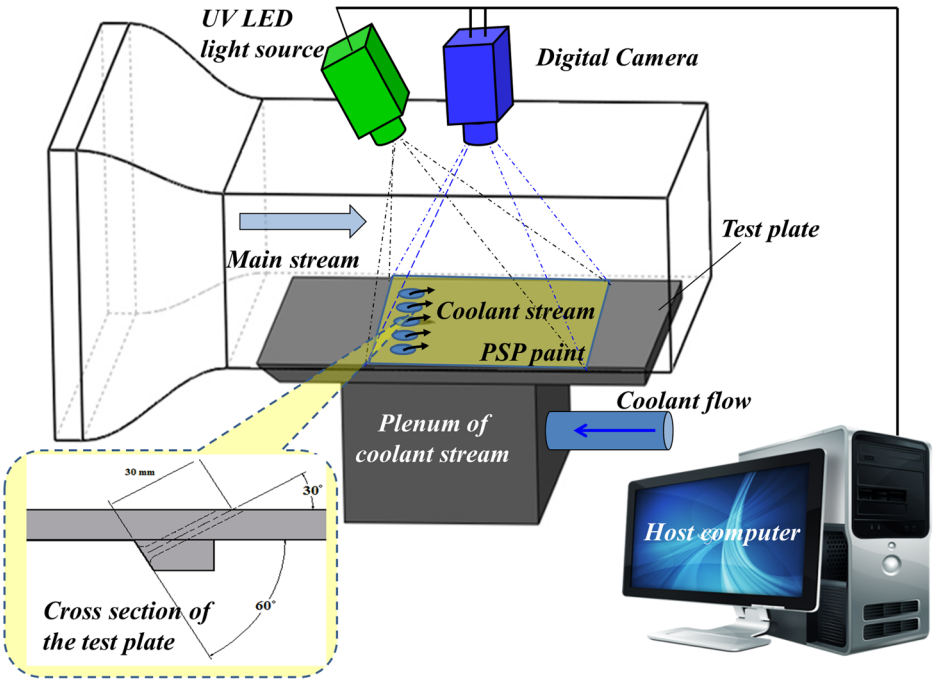

Fig. 3 Experimental setup for the film cooling measurements by using PSP technique

element mass flow meter, which provides the standard volumetric flow rate in standard liters per minute (SLPM). The flow meter is capable of compensating the temperature and absolute pressure conditions within the coolant line to the laboratory temperature and pressure conditions to obtain the appropriate SLPM at the laboratory conditions. It also measures the absolute pressure to within 0.01 psia and the absolute temperature to within 0.01 °C and resolves the flow rate to within 0.1 SLPM. It can be used with a number of different gases—including air, N_2, CO_2, and others—by accounting for the viscosity of the gas in the laminar flow calculation. Based on the manufacturer's quote of the bias uncertainty B_Q of the flowmeter, and measured values of precision uncertainty S_Q, the absolute and relative uncertainties in Q are listed in Table 1 for the maximum and minimum CO_2 flowrates investigated in this study.

Analysis of the Measurement Uncertainty

As reported in the recent work of Johnson et al. [18], the film cooling effectiveness data based on the PSP measurements have been compared quantitatively against those of Baldauf et al. [2] with an IR thermometry technique at comparable test conditions. The measured film cooling effectiveness data with the PSP technique were found to agree well with those derived directly from the temperature-based measurements. The analysis given herein will focus mainly on the measurement uncertainty and process uncertainty of the PSP measurements and evaluate various associated uncertainties on the measured film cooling effectiveness distributions over the surfaces of interest, because those sources of uncertainty that are most commonly encountered when the PSP technique is used to determine the adiabatic film cooling effectiveness distribution.

Table 1 Uncertainties of the Omega FMA-1600 mass flow meter when used with the five-hole test coupon and CO_2 as the coolant gas

Blowing ratio, M	Q (SLPM)	B_Q (SLPM)	S_Q (SLPM)	U_Q (SLPM)	U_Q/Q
0.40 (minimum flow)	46.0	1.4	0	1.4	0.030
2.50 (maximum flow)	288.7	2.8	2	3.5	0.012

Certain system and bias errors are not included in this study, such as decay of the PSP painting, which is dependent upon the chemistry of the luminophore and is therefore not under the control of most investigators. To satisfy their own curiosity, the authors confirmed that the decay of PSP emission is insignificant even under excitation times on the order of hours, which excludes such concern for typical studies of the film cooling effectiveness (i.e., PSP measurements can usually be completed on the order of a few minutes' excitation). Repeatability of our measurements has been investigated, though is not an emphasis of this study. Neither are systematic errors considered that depend on the light source and image acquisition available to the users, such as those related to timing optimization, etc. It was confirmed that our measured image intensities are linear in the range of the exposure times that we did use.

Figure 4 shown the image intensity distributions of the four acquired images for the film cooling effectiveness measurements by using the PSP technique, which are the background image acquired with the excitation light off at nonflow condition (i.e., I_b), reference image acquired with the excitation light on at nonflow condition (i.e., I_{ref}), acquired PSP image with airflow being used as the coolant stream (i.e., I_{air}), and the acquired PSP image with the oxygen-free gas (i.e., CO_2 for the present study) as the coolant stream (i.e., I_{gas}), respectively. It was found that the typical values for each of the image exposures are $I_b \sim 117$ counts, $I_{ref} \sim 700$ counts, $I_{air} \sim 700$ counts, and $I_{gas} \sim 700$–1200 counts throughout the main portion of the region of interest. This flow scenario is the case where density ratio, DR = 1.53, and blowing ratio, $M = 0.85$, and is chosen here as a representative case for the present study. These images are ensemble averages of 65 exposures, 100 exposures, 130 exposures, and 500 exposures for the four images I_b, I_{ref}, I_{air}, and I_{gas}, respectively, which were confirmed to be long enough sample records for the RMS statistics of each image to converge. The exposure time was set such that the image intensities on this order were achieved because (a) these intensities are high enough that the quantum efficiency becomes unimportant in the uncertainty analysis, and (b) the exposure times needed to achieve these intensities were still brief enough to

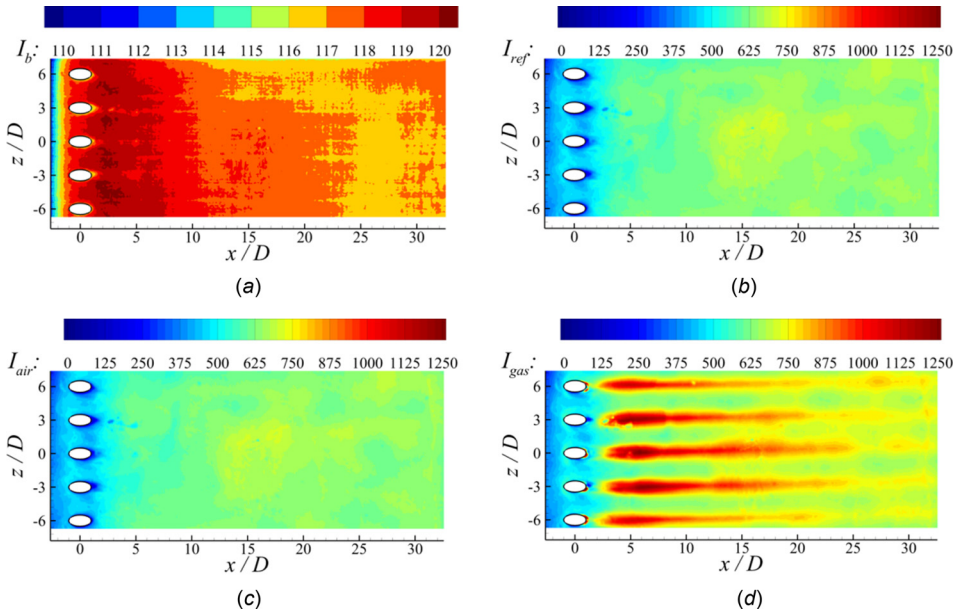

Fig. 4 Mean intensity maps of the four ensemble-averaged image intensity maps. Units are in terms of image intensity counts, which is a multiple of electrons freed by photons incident upon the CCD array. (*a*) I_b, (*b*) I_{ref}, (*c*) I_{air}, (*d*) I_{gas}.

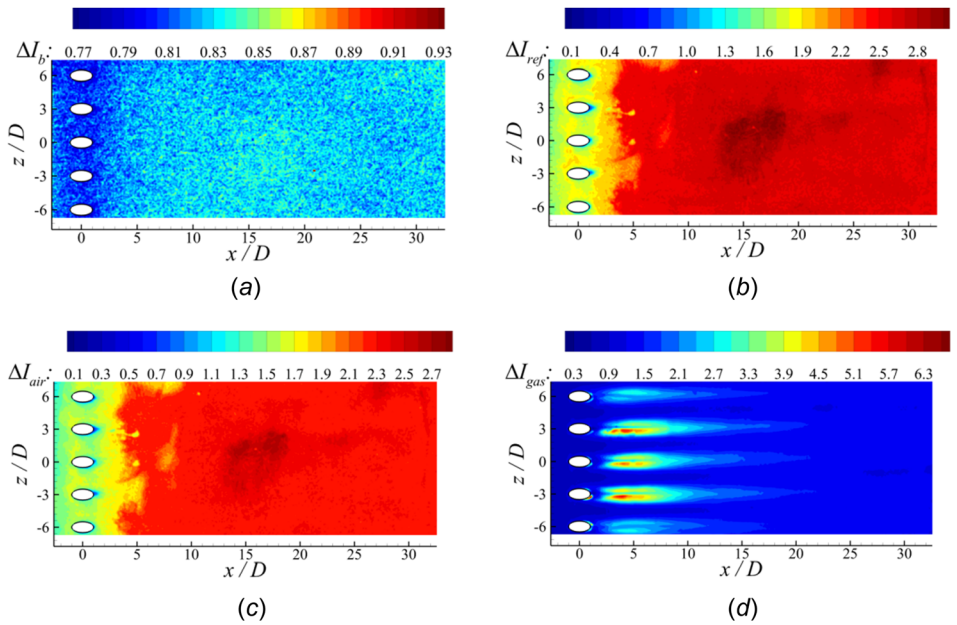

Fig. 5 Confidence interval maps of the intensity distributions of the four acquired images. Units are in terms of image intensity counts, which is a multiple of electrons freed by photons incident upon the CCD array. (*a*) ΔI_b, (*b*) ΔI_{ref} (*c*) ΔI_{air}, (*d*) ΔI_{gas}.

allow rapid collection of large ensembles of images. Figure 5 gives the relative precision uncertainty in terms of the confidence intervals for the image ensembles, assuming normal distribution. It is noted that I_b has a precision uncertainty of less than 1 count (i.e., noise level about 0.7%) throughout the entire region of interest. For the reference and air-as-coolant images I_{ref} and I_{air}, the absolute precision uncertainty is only 2–4 counts for a relative uncertainty of about 0.4%. For the I_{gas} image, the precision uncertainty ranges from 2 to 20 counts; for the majority of the region of interest—everywhere beyond $x/D = 10$—the confidence interval is about 7 counts for a relative precision uncertainty of roughly 0.6%. A typical value for the precision uncertainty near the centerline of the middle hole is about 5 counts in a region, where the mean intensity is ~1250 counts, i.e., for 0.4% relative uncertainty. In the far field it is observed that the relative precision uncertainty is quite low at less than 0.4% for all images, and less than 0.2% for the I_{gas} image.

The measurement technique depends on passing normalized image intensity maps through a calibration curve to determine normalized ratios of the partial oxygen pressure. These normalized intensity maps are computed in the following manner:

$$I^*_{air} \equiv (I_{ref} - I_b)/(I_{air} - I_b) \tag{9}$$

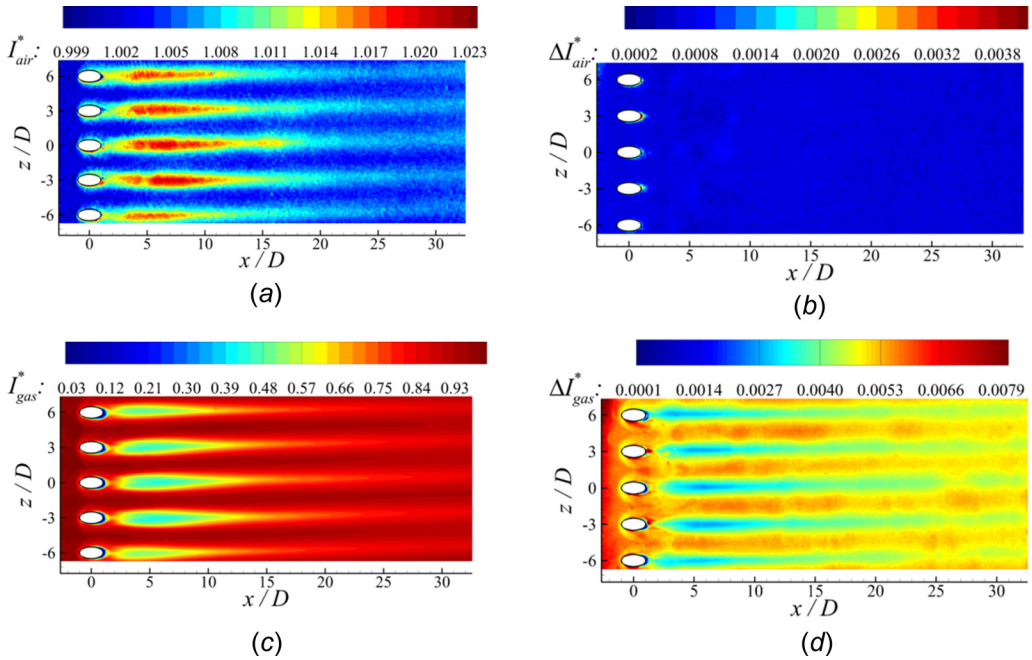

Fig. 6 Image intensity ratios and their corresponding uncertainty. (*a*) I^*_{air}, (*b*) ΔI^*_{air}, (*c*) I^*_{gas}, (*d*) ΔI^*_{gas}.

$$I^*_{gas} \equiv (I_{ref} - I_b)/(I_{gas} - I_b) \tag{10}$$

where I_b is removed from I_{ref}, I_{air}, and I_{gas} to negate effects of dark current and infiltration of ambient light into the measurement domain; essentially, I_b is a fixed intensity bias. It is necessary to compute the total measurement uncertainties of the image intensity ratios I^*_{air} and I^*_{gas}: U_{I^*air} and U_{I^*gas}, respectively. Following the Taylor series method for estimating propagation of uncertainty described in Ref. [24], the total measurement uncertainty in I^*_{air} and I^*_{gas} are

$$(U_{I^*\,air})^2 = \left(\frac{\partial I^*_{air}}{\partial I_{air}} S_{I\,air}\right)^2 + \left(\frac{\partial I^*_{air}}{\partial I_b} S_{I\,b}\right)^2 + \left(\frac{\partial I^*_{air}}{\partial I_{ref}} S_{I\,ref}\right)^2 \tag{11}$$

$$(U_{I^*\,gas})^2 = \left(\frac{\partial I^*_{gas}}{\partial I_{gas}} S_{I\,gas}\right)^2 + \left(\frac{\partial I^*_{gas}}{\partial I_b} S_{I\,b}\right)^2 + \left(\frac{\partial I^*_{gas}}{\partial I_{ref}} S_{I\,ref}\right)^2 \tag{12}$$

where S_i is the precision uncertainty of variable i. Figure 6 gives the computed intensity ratios and their relative uncertainties. The intensity ratio I^*_{air} is nearly unity throughout the entire painted measurement domain, with a value of roughly 1.02 in the near-field and a value of 1.00 elsewhere in the region of interest. The absolute and relative uncertainties are valued at about ± 0.02, or $\pm 2\%$. The other intensity ratio I^*_{gas} ranges from 0.44 to 1.00 in the region of interest. The corresponding absolute uncertainty values range from ± 0.002 to ± 0.010 throughout the region of interest.

PSP Calibration Uncertainty

The next step in the PSP measurement process is to convert the intensity ratios to normalized oxygen pressure ratios through use of the PSP calibration, which is shown in Fig. 2. The calibration was performed for five different temperature conditions. Based on the $P^* - I^*$ relationship shown in Fig. 2, the five temperature conditions were used to determine the precision uncertainty of the calibration curve, which is 0.9% or less at a confidence of 95% using the Student's t-distribution. Thus, it is shown that $P^* - I^*$ relationship is quite insensitive to temperature effects, provided the images are normalized with a reference image taken at the same temperature condition, as they were for these calibration runs and for the wind tunnel experiments as well.

Uncertainty in the calibration was performed by determining error bars of pressure and image intensity for each calibration data point. The calibration data $[(I^*)_i, (P^*)_i]$ were then plotted and a calibration curve fit to them. Additionally, calibration curves P^{*-} and P^{*+} were also fit to the limiting extents of the error bars $[(I^* + U_{I^*})_i, (P^* - U_{P^*})]$ and $[(I^* - U_{I^*})_i, (P^* + U_{P^*})]$, respectively. The calibration curve was then analyzed in the same manner demonstrated in Fig. 7, where the range in variation of uncertainty in P^* is determined as

$$S_{P^*} = \frac{1}{2}\left[P^{*+}(I^* - S_{I^*}) - P^{*-}(I^* + S_{P^*})\right] \tag{13}$$

The end result of this analysis is a lookup table for measurement uncertainty where by S_{P^*}/P^* is found as a function of I^* with S_{I^*} as a parameter, as shown in Fig. 8. The relative uncertainty in P^* reaches as high as 3.6% at low I^* values where S_{I^*} is high, such as in the near-field edge regions of certain coolant

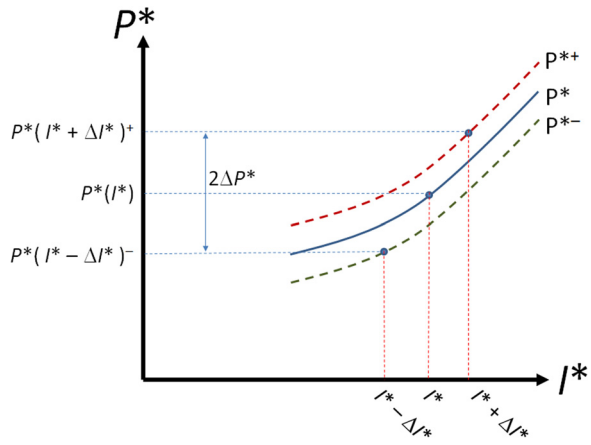

Fig. 7 Uncertainty propagation through the PSP calibration curve. Bounding curves are determined by the error bars (uncertainty) of the discrete calibration data points.

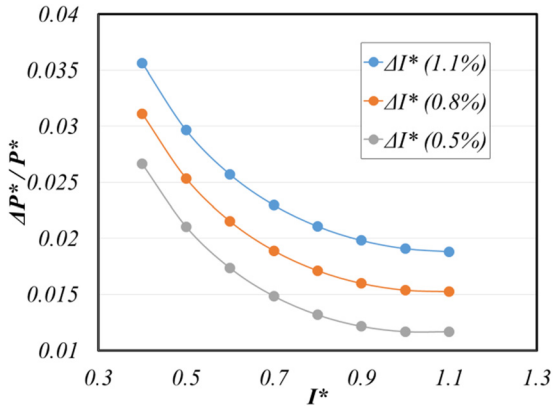

Fig. 8 Uncertainty in the PSP pressure measurement; $\Delta P^*/P^*$ is a function of I^* with ΔI^* as a parameter

streams. Typical values of P^*_{air} are approximately unity, ranging from 0.999 in most of the near and far field to local maxima as high as 1.011 in the near field close to the hole outlets. Based on the measurement results given in Fig. 6, the relative uncertainty S_{P^*air}/P^*_{air} ranges from 1.3% to 1.6%, depending on location on the test plate. As shown in Fig. 9, the absolute uncertainty U_{P^*air} is approximately the same value because P^*_{air} is so close to unity everywhere. For the measurements where the coolant gas is used, P^*_{gas} ranges from a low of about 0.28 in the near field to 0.75 in the far field. The relative uncertainty U_{P^*gas}/P^*_{gas} is as high as 6.0% locally in the near field at the edges of certain coolant streams and about 4.0–4.5% near the centerline of the coolant streams within the first $x/D < 5$ or so. Beyond $x/D = 5$, the relative uncertainty falls to about 3% and beyond $x/D = 10$, it is about 1.6% everywhere. The next step in the data reduction is to take the ratio of P^*_{air} to P^*_{gas}: $P^*_{ratio} \equiv P^*_{air}/P^*_{gas} = P_{air}/P_{gas}$. The propagation of measurement uncertainty through this ratio is easily calculated using the Taylor series method

$$(U_{P*\text{ratio}})^2 = \left(\frac{\partial P^*_{\text{ratio}}}{\partial P^*_{\text{gas}}} U_{P*\text{gas}}\right)^2 + \left(\frac{\partial P^*_{\text{ratio}}}{\partial P^*_{\text{air}}} U_{P*\text{air}}\right)^2 \tag{14}$$

Figure 9(*c*) gives the distribution of the resulting measurement error in the pressure ratio $U_{\text{Pair/Pgas}}$. It can be seen that the resulting error is about 3% locally in the near-field coolant stream and less than 2% in the far field.

Conversion to Film Cooling Effectiveness

As described above, the measured pressure ratio distribution can be converted to film cooling effectiveness map by using Eq. (2) and the results are shown in Fig. 10. Note that the effectiveness pattern here resembles an inverse pattern of the I^*_{gas} contour map shown in Fig. 6(*c*). The corresponding uncertainty, also shown in Fig. 10, is given by

$$U_\eta = \pm \left| \frac{d\eta}{d(P_{\text{air}}/P_{\text{gas}})} U_{P_{\text{air}}/P_{\text{gas}}} \right| \tag{15}$$

This expression assumes the uncertainty in MW is negligible, which is reasonable for the measurements where highly pure N_2 or CO_2 were used as the coolant gas. The sensitivity to errors in P^*_{ratio} is given as follows:

$$\frac{d\eta}{d(P_{\text{air}}/P_{\text{gas}})} = \frac{\text{MW}}{\left\{\left[\left(\frac{P_{\text{air}}}{P_{\text{gas}}}\right) - 1\right]\text{MW} + 1\right\}^2} \tag{16}$$

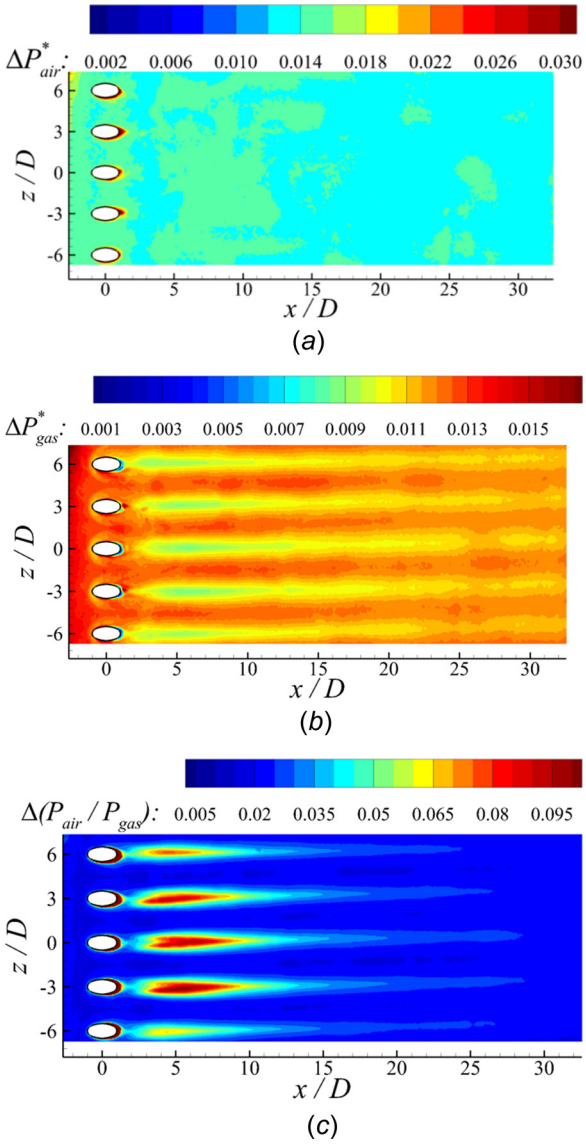

Fig. 9 Measurement uncertainties of normalized pressure measurements. (*a*) ΔP^*_{air}, (*b*) ΔP^*_{gas}, (*c*) $\Delta(P^*_{air}/P^*_{gas})$.

For the relevant range of P_{air}/P_{gas} (i.e., $1 < P_{air}/P_{gas} < 3.3$), the sensitivity is shown in Fig. 11. The sensitivity is parameterized by MW. For values of P_{air}/P_{gas} less than about 1.7, the sensitivity is strongly dependent on MW. For higher P_{air}/P_{gas}, the sensitivity is nearly independent of MW; this region is shown in the line contour in Fig. 11. In this example, as mentioned previously, measurements are made using CO_2 (DR = 1.53) as the coolant gas. Because the near field generally has higher relative error in P_{air}/P_{gas} than does the far field applying the effectiveness conversion actually makes the uncertainty field U_η somewhat *more* uniform than it is for $U_{P_{air}/P_{gas}}$. As shown in Fig. 10, the measurement uncertainty U_η ranges from about ±0.03 in the far field to ±0.08 in the reattachment region of the near field where η is highest.

Process and Total Uncertainty

Now that the measurement uncertainty has been described, it is important to consider the effect that uncertainty in the experimental parameters has upon the total uncertainty of the effectiveness field. The primary parameter that was used in the experiments is

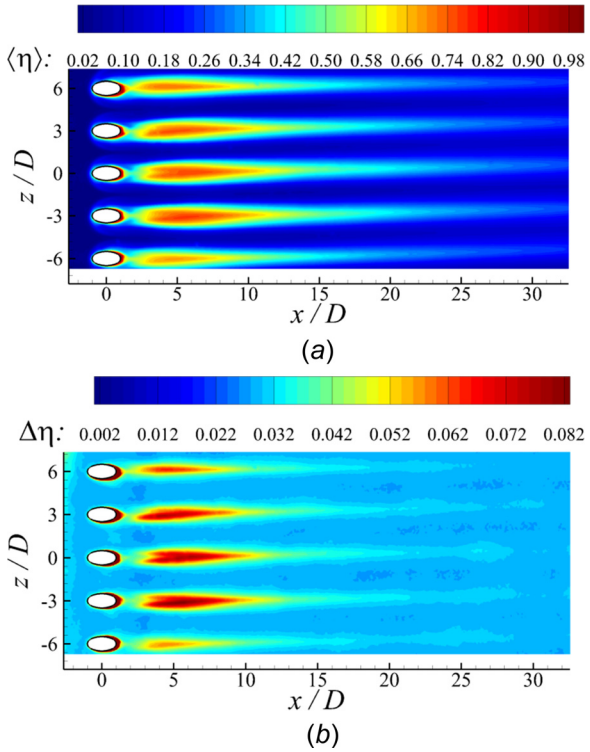

Fig. 10 Measured film cooling effectiveness distribution and measurement uncertainty map. (*a*) The film cooling effectiveness measurement result under analysis and (*b*) Measurement uncertainty in the film cooling effectiveness.

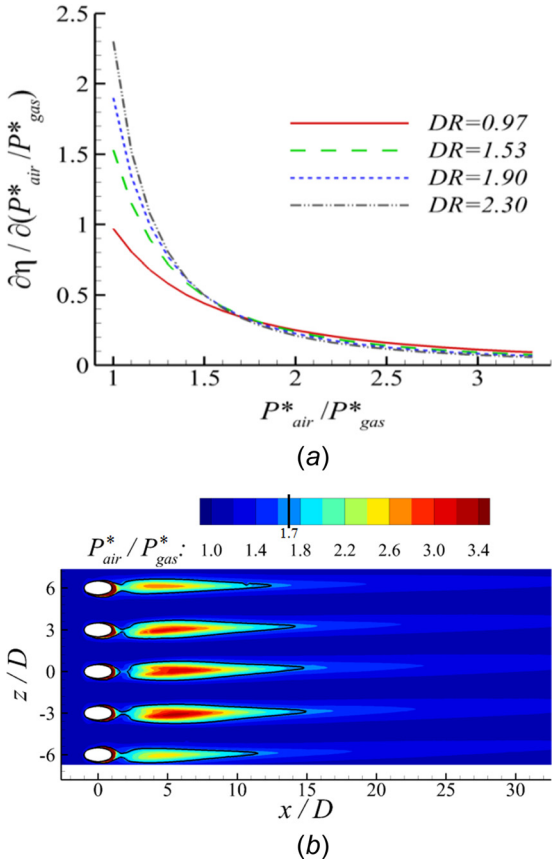

Fig. 11 Sensitivity analysis of the film cooling effectiveness to the pressure ratio. (*a*) The sensitivity of the film cooling effectiveness to the pressure ratio and (*b*) The pressure ratio measurement, with line contour indicating the region where DR does not affect uncertainty.

the blowing ratio, which is defined as the ratio of the mass fluxes of the coolant stream to the mainstream flow

$$M = \frac{(\rho V)_{\text{coolant}}}{(\rho U)_{\infty}} = \text{DR}\,\frac{V_{\text{coolant}}}{U_{\infty}} \tag{17}$$

The corresponding uncertainty in M is

$$\frac{U_M}{M} = \sqrt{\left(\frac{U_V}{V}\right)^2 + \left(\frac{U_U}{U}\right)^2 + \left(\frac{U_{\text{DR}}}{\text{DR}}\right)^2} \tag{18}$$

Note that for a high-purity coolant gas such as CO_2 (minimum of 99.99% purity was used for this study), the DR is considered a well-known constant and U_{DR} is negligible compared to the uncertainty of other parameters. The relative uncertainty in free-stream velocity U_∞ is approximately 2%, and is dominated by the uncertainty in Pitot-static probe alignment while the relative uncertainty in V_{coolant} ranges from about 4.3% at low M to 1.3% for high M cases, which is dominated by the instrument bias quoted by the manufacturer. For completeness, the error in manufacturing the coolant hole diameter was investigated and it was found that the diameters tend to be oversized by a small amount (about +0.02 mm larger than the specified diameter of 5.00 mm), which remains a negligible error compared to the mass flow meter bias. Nonetheless, the relative error in M for pure coolant experiments ranges from 2.4% for high blowing rate experiments to 4.7% at low blowing rates. In order to relate the uncertainty in M to an overall uncertainty in η, a sensitivity of $\partial\eta/\partial M$ is estimated such that

$$(U_\eta)_{\text{process}} = \frac{\partial \eta}{\partial M} U_M \tag{19}$$

The sensitivity is computed using effectiveness maps measured at successive blowing rates using the central difference method with a data set of $M = 0.50$, 0.60, 0.85, 1.00, and 1.20. Plots of the sensitivity $\partial\eta/\partial M$ are shown in Fig. 12 for three values of M that were tested. Typical values of uncertainty in η due to process errors are ± 0.04 in the near field for $M = 0.60$; for higher M, the near-field error decreases in magnitude, peaking at about $(U_\eta)_{\text{process}} = \pm 0.02$ for $M = 1.20$. In the far field, the process uncertainty is quite low at less than 0.016 in magnitude for most of the values of M that we tested. For the $M = 0.85$ case that is being highlighted here, the process uncertainty peaks at about $(U_\eta)_{\text{process}} = \pm 0.04$ at certain near-field locations, mainly at the lateral leading edges of the reattachment region of the coolant stream. In the far field the process uncertainty tapers down to very near zero, with $(U_\eta)_{\text{process}} < \pm 0.01$ virtually everywhere beyond $x/D = 12$.

The root-sum-square method was used to combine the effects of process uncertainty with the measurement uncertainty. The resulting total uncertainty $(U_\eta)_{\text{total}}$ is shown in Fig. 13 for the $M = 0.85$ case. Total uncertainty in the reattachment region peaks at about $(U_\eta)_{\text{total}} = \pm 0.09$ while far-field uncertainty is fairly uniform at a value of about $(U_\eta)_{\text{total}} = \pm 0.03$. Commonly, the film cooling effectiveness is reported in terms of the laterally averaged effectiveness, found by

$$\langle \eta \rangle_{|z|<L} = \frac{1}{2L}\int_{-L}^{-L} \eta \cdot dz \tag{20}$$

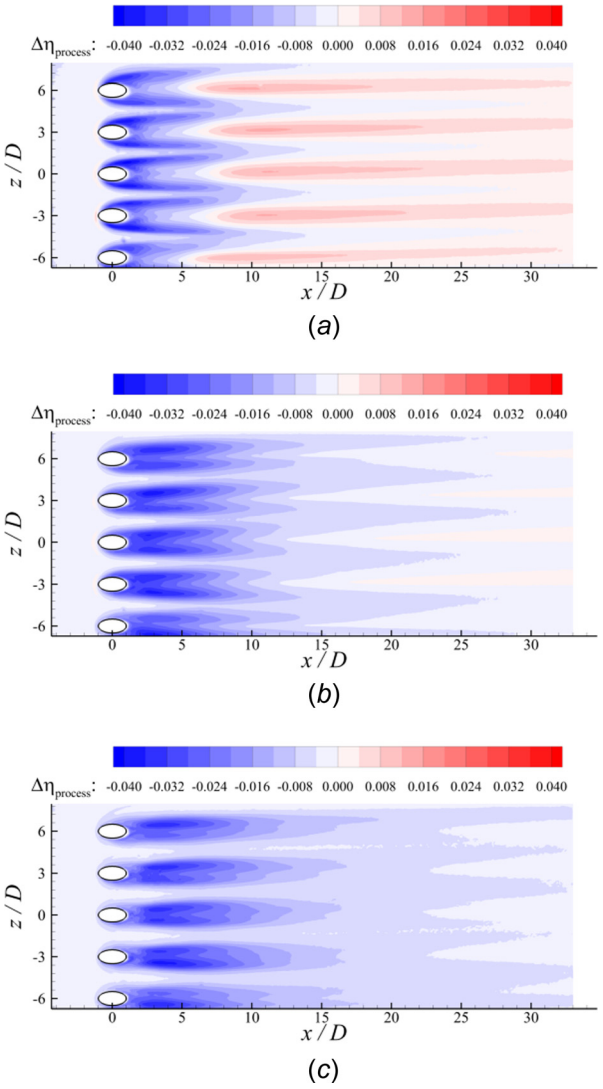

Fig. 12 Process uncertainty maps made by discrete derivative estimation for the test cases with different bowling ratios. (*a*) $M = 0.60$, (*b*) $M = 0.85$, and (*c*) $M = 1.00$.

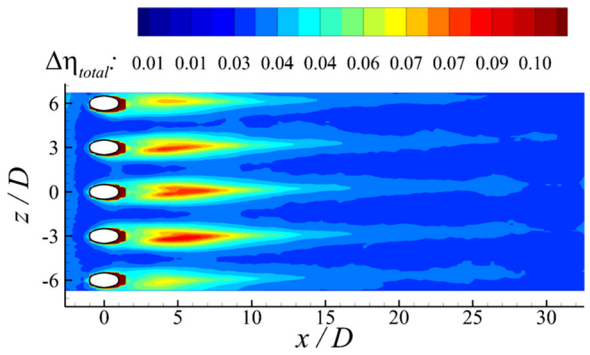

Fig. 13 The total uncertainty in effectiveness $\Delta\eta_{total}$, accounting for both process and measurement uncertainty

where the lateral averaging domain is typically some integer multiple of the lateral pitch spacing between adjacent coolant holes. In the present study, $L = 3D$ is the lateral pitch spacing. For discrete measurements of the film cooling effectiveness, the uncertainty in the laterally averaged effectiveness reduces to the formula

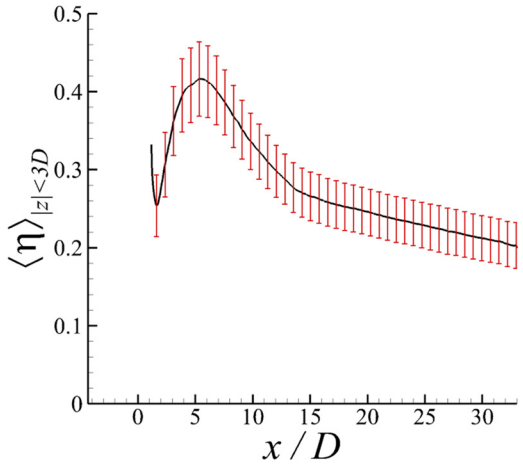

Fig. 14 Uncertainty in the laterally averaged film cooling effectiveness

$$\Delta\langle\eta\rangle_{|z|<L} = \frac{1}{N-1}\sum_{i=1}^{N}\Delta\eta\cdot(z_i - z_{i-1}) \tag{21}$$

which directly results from the root-sum-square method of uncertainty propagation, obtained from the discretization of the integral in Eq. (20). The laterally averaged film cooling effectiveness with error bars showing the total uncertainty is shown in Fig. 14. The magnitude of the uncertainty peaks at $U\eta_{|z|<L} = 0.05$ in the reattachment region, around $x/D = 6$. In the far field it holds a nearly constant value of $U\eta_{|z|<L} = 0.03$.

Conclusions

In the present study, a comprehensive uncertainty analysis is performed to assess measurement uncertainty and process uncertainty of the PSP measurements and to evaluate the associated uncertainties on the measured film cooling effectiveness distributions over the surfaces of interest by using the PSP technique with a mass transfer analog to traditional thermal-based measurements. The experimental study was conducted in a low-speed wind tunnel under an isothermal condition. While airflow was used to represent the hot mainstream flow, CO_2 gas with a density ratio of $DR = 1.5$ was supplied to simulate the coolant stream for the PSP measurements to map the adiabatic film cooling effectiveness distribution over a flat test plate with an array of five cylindrical coolant holes.

For the particular flow scenario in question, the PSP film cooling effectiveness measurement technique has a varying degree of uncertainty throughout the measurement domain. Based on the estimates of measurement uncertainty made herein, a fair estimate for the near field absolute uncertainty is about $U_\eta = \pm 0.08$ in the near field where the coolant stream reattaches to the plate and the effectiveness is near its maximum. In the far field the measurement uncertainty is about $U_\eta = \pm 0.03$, with little spatial variation in the uncertainty field. Considering process uncertainty, for the particular case of interest ($M = 0.85$, $DR = 1.53$) the blowing rate has an uncertainty of $U_M = 0.02$, which results in a process uncertainty that peaks at $(U_\eta)_{process} = \pm 0.04$ in the reattachment region of the near field tapering to insignificance in the far field. The combination of the measurement uncertainty and the process uncertainty through the root-sum-square method gives the total uncertainty. In the near field the total uncertainty reaches its greatest value at $(U_\eta)_{total} = 0.09$; in the far field where process uncertainty is determined to have a negligible effect, $(U_\eta)_{total} = 0.03$ nearly everywhere. The flow field in the far field is characterized by weaker fluctuations than near the coolant holes, and in that same spirit, the PSP output is generally much steadier

in this region, which allows a more reliable measurement in the far field than the near field. Thus, it would seem that PSP technique is most ideally suited for absolute effectiveness measurements in regions of stable flow. For comparison, the temperature-sensitive paint (TSP) technique carried out by Kunze et al. [9] quotes relative uncertainties on the order of 4% for $\eta = 0.8$ and 10% for $\eta = 0.3$. A comparison to the uncertainties of other methods would be of some use (IR thermography, TSP, etc), with citations to some representative papers regarding those methods.

Acknowledgment

The authors would like to thank Bill Rickard, Andrew Jordan, and Jim Benson of Iowa State University for their technical support and expertise throughout this study. Grateful acknowledgements also go to Mr. Marc Regan, Mr. Mark Johnson, and Mr. Omar Longuo of Iowa State University for their assistance with setup and conduction of the experiments.

Appendix: "Best Practice" for Film Cooling Effectiveness Measurements With PSP Technique

The best practices for minimizing errors in determining the adiabatic film cooling effectiveness based on PSP measurements is suggested as follows:

Before conducting experiments, it must be confirmed what range of intensity values the camera can gather while still yielding a linear response. This test can be done simply by imaging a fixed object at many different exposure times and plotting the intensity versus exposure time for the brightest part of the image.

For calibration, an imaging cell that can be temperature- and pressure-regulated is necessary, and extreme diligence should be taken to remove all sources of ambient light from the cell during calibration. The background and reference images must be taken at precisely the same temperature as the rest of the calibration images; a temperature detector that can resolve to at least tenths of a degree should be used to measure the temperature inside the calibration cell. Because certain PSP formulations may be susceptible to photo-degradation, the excitation light should be activated only during image acquisition.

It is advised that the calibration sample be painted very carefully according to the manufacturer's instructions, and that only a region of the test coupon where the PSP is rather uniform should be used for calibration analysis. The PSP should be carefully applied using a clean airbrush, and the user should practice extensively in order to achieve a high degree of consistency when painting test coupons. A large ensemble of images should be taken and the results averaged. Likewise, the pressure should be recorded with a high degree of accuracy and averaged over many samples. The calibration should be done on a surface that is free of vibrations. The camera, light source, and any shrouding must not be disturbed during calibration. Similar levels of care must also be taken during the experimentation phase.

Perhaps, the greatest source of frustration that the authors encountered during the experiment phase was controlling ambient light sources and preventing even small disturbances to the camera and light mounts. Here again, if a shroud is used to isolate the test section from ambient light, extreme care must be taken to ensure that the shroud remains perfectly still during all the tests, as well as the camera and excitation light. The experiment should be set up such that all vibration is isolated, the camera and light and test coupons are all rigidly mounted, and no vibrations or air currents may disturb the shrouding.

During the experiment phase, the camera must be carefully focused in some way without risk of scratching of the PSP from the test coupon. No images should be taken until the light source has achieved thermal equilibrium such that its output becomes steady. Because the image intensity is greatest for the coolant gas images, the exposure time should be set by taking sample images with the coolant gas flowing. For simple circular holes, the intensity tends to be highest for low blowing ratios, whereas the shaped holes the intensity tends to be highest at larger blowing ratios. By taking test images at the appropriate highest-intensity blowing ratio, the exposure time can be set such that the camera response remains linear everywhere in the image field for all test cases.

References

[1] Baldauf, S., Schulz, A., and Wittig, S., 2001, "High-Resolution Measurements of Local Heat Transfer Coefficients From Discrete Hole Film Cooling," ASME J. Turbomach., **123**(4), pp. 749–757.

[2] Baldauf, S., Schulz, A., and Wittig, S., 2001, "High-Resolution Measurements of Local Effectiveness From Discrete Hole Film Cooling," ASME J. Turbomach., **123**(4), pp. 758–765.

[3] Wright, L. M., Gao, Z., Varvel, T. A., and Han, J.-C., 2005, "Assessment of Steady State PSP, TSP, and IR Measurement Techniques for Flat Plate Film Cooling," ASME Paper No. HT2005-72363.

[4] Han, J.-C., Dutta, S., and Ekkad, S., 2012, *Gas Turbine Heat Transfer and Cooling Technology*, 2nd ed., CRC Press, Boca Raton, FL.

[5] Silieti, M., Kassab, A. J., and Divo, E., 2009, "Film Cooling Effectiveness: Comparison of Adiabatic and Conjugate Heat Transfer CFD Models," Int. J. Therm. Sci., **48**(12), pp. 2237–2248.

[6] Knost, D. G., and Thole, K. A., 2003, "Computational Predictions of Endwall Film-Cooling for a First Stage Vane," ASME Paper No. GT2003-38252.

[7] Saumweber, C., Schulz, A., and Wittig, S., 2002, "Free-Stream Turbulence Effects on Film Cooling With Shaped Holes," ASME Paper No. GT2002-30170.

[8] Chyu, M. K., Hsing, Y. C., and Bunker, R. S., 1998, "Measurements of Heat Transfer Characteristics of Gap Leakage Around a Misaligned Component Interface," ASME Paper No. 98-GT-132.

[9] Kunze, M., Preibisch, S., Vogeler, K., Landis, K., and Heselhaus, A., 2008, "A New Test Rig for Film Cooling Experiments on Turbine Endwalls," ASME Paper No. GT2008-51096.

[10] Pedersen, D. R., Eckert, E. R. G., and Goldstein, R. J., 1977, "Film Cooling With Large Density Differences Between the Mainstream and the Secondary Fluid Measured by the Heat-Mass Transfer Analogy," ASME J. Heat Transfer, **99**(4), p. 620.

[11] Zhang, L. J., and Jaiswal, R. S., 2001, "Turbine Nozzle Endwall Film Cooling Study Using Pressure-Sensitive Paint," ASME J. Turbomach., **123**(4), p. 730.

[12] Ahn, J., Mhetras, S., and Han, J., 2005, "Film-Cooling Effectiveness on a Gas Turbine Blade Tip Using Pressure-Sensitive Paint," ASME J. Heat Transfer, **127**(5), pp. 521–530.

[13] Charbonnier, D., Ott, P., Jonsson, M., Cottier, F., and Koübke, T., 2009, "Experimental and Numerical Study of the Thermal Performance of a Film Cooled Turbine Platform," ASME Paper No. GT2009-60306.

[14] Yang, Z., and Hu, H., 2011, "Study of Trailing-Edge Cooling Using Pressure Sensitive Paint Technique," J. Propul. Power, **27**(3), pp. 700–709.

[15] Yang, Z., and Hu, H., 2012, "An Experimental Investigation on the Trailing Edge Cooling of Turbine Blades," Propul. Power Res., **1**(1), pp. 36–47.

[16] Rallabandi, A. P., Grizzle, J., and Han, J.-C., 2011, "Effect of Upstream Step on Flat Plate Film-Cooling Effectiveness Using PSP," ASME J. Turbomach., **133**(4), p. 041024.

[17] Zhang, L. J., and Fox, M., 1999, "Flat Plate Film Cooling Measurement Using PSP and Gas Chromatograph Techniques," 5th ASME/JSME Thermal Engineering Joint Conference, San Diego, CA, Mar. 14–19, American Society of Mechanical Engineers, New York.

[18] Johnson, B., Tian, W., Zhang, K., and Hu, H., 2014, "An Experimental Study of Density Ratio Effects on the Film Cooling Injection From Discrete Holes by Using PIV and PSP Techniques," Int. J. Heat Mass Transfer, **76**, pp. 337–349.

[19] Natsui, G., Little, Z., Kapat, J. S., Dees, J. E., and Laskowski, G., 2015, "A Detailed Uncertainty Analysis of Adiabatic Film Cooling Effectiveness Measurements Using Pressure Sensitive Paint," ASME Paper No. GT2015-42707.

[20] Liu, T., and Sullivan, J. P., 2005, *Pressure and Temperature Sensitive Paints*, Springer-Verlag, Berlin, Germany.

[21] Wright, L. M., McClain, S. T., and Clemenson, M. D., 2011, "Effect of Density Ratio on Flat Plate Film Cooling With Shaped Holes Using PSP," ASME J. Turbomach., **133**(4), p. 041011.

[22] Han, J.-C., and Rallabandi, A., 2010, "Turbine Blade Film Cooling Using PSP Technique," Front. Heat Mass Transfer, **1**(1), p. 013001.

[23] Liu, K., Yang, S.-F., and Han, J.-C., 2012, "Influence of Coolant Density on Turbine Blade Film-Cooling With Axial Shaped Holes," ASME Paper No. HT2012-58144.

[24] Coleman, H., and Steele, W., 2009, *Experimentation, Validation, and Uncertainty Analysis for Engineers*, Wiley, New York.